



# Ecosystem-Scale Oxygen Manipulations Alter Terminal Electron Acceptor Pathways in a Eutrophic Reservoir

Ryan P. McClure,<sup>1\*</sup> Madeline E. Schreiber,<sup>2</sup> Mary E. Lofton,<sup>1</sup> Shengyang Chen,<sup>3</sup> Kathryn M. Krueger,<sup>2</sup> and Cayelan C. Carey<sup>1</sup>

<sup>1</sup>Department of Biological Sciences, Virginia Tech, Blacksburg, Virginia 24061, USA; <sup>2</sup>Department of Geosciences, Virginia Tech, Blacksburg, Virginia 24061, USA; <sup>3</sup>UNSW Water Research Laboratory, UNSW Sydney, 110 King St, Manly Vale, New South Wales 2093, Australia

## ABSTRACT

Lakes and reservoirs globally are experiencing unprecedented changes in land use and climate, depleting dissolved oxygen (DO) in the bottom waters (hypolimnion) of these ecosystems. Because DO is the most energetically favorable terminal electron acceptor (TEA) for organic carbon mineralization, its availability controls the onset of alternate TEA pathways (for example, denitrification, manganese reduction, iron reduction, sulfate reduction, methanogenesis). Low DO concentrations can trigger organic carbon mineralization via alternate TEA pathways in the water column and sediments, which has important implications for greenhouse gas production [carbon dioxide (CO<sub>2</sub>) and methane (CH<sub>4</sub>)]. In this study, we experimentally injected supersaturated DO into the hy-

polimnion of a eutrophic reservoir and measured concentrations of TEAs and terminal electron products (TEPs) in the experimental reservoir and an upstream reference reservoir. We calculated the electron equivalents yielded from each TEA pathway and estimated the contributions of each TEA pathway to organic carbon processing in both reservoirs. DO additions to the hypolimnion of the experimental reservoir promoted aerobic respiration, suppressing most alternate TEA pathways and resulting in elevated CO<sub>2</sub> accumulation. In comparison, organic carbon mineralization in the reference reservoir's anoxic hypolimnion was dominated by alternate TEA pathways, resulting in both CH<sub>4</sub> and CO<sub>2</sub> accumulation. Our ecosystem-scale experiments demonstrate that the alternate TEA pathways that succeed aerobic respiration in lakes and reservoirs can be manipulated at the ecosystem scale. Moreover, changes in the DO dynamics of freshwater lakes and reservoirs may result in concomitant changes in the redox reactions in the water column that control organic carbon mineralization and greenhouse gas accumulation.

Received 16 June 2020; accepted 22 October 2020;  
published online 23 November 2020

**Electronic supplementary material:** The online version of this article (<https://doi.org/10.1007/s10021-020-00582-9>) contains supplementary material, which is available to authorized users.

**Author contributions** CCC conceived the original research project. RPM and CCC worked closely together to develop the original research ideas addressed in this paper. RPM and MES led the overall synthesis and interpretation of the data and writing with many contributions from CCC. RPM, MEL, SC, and KMK collected field data, and RPM, SC, MEL, KMK, and CCC compiled and analyzed data. All authors approved the final version of the manuscript.

\*Corresponding author; e-mail: ryan333@vt.edu

**Key words:** Anoxia; Carbon dioxide; Dissolved oxygen; Greenhouse gases; Hypolimnetic oxygenation; Methane; Redox reactions; Terminal electron acceptor pathways; Whole-ecosystem experiment.

## HIGHLIGHTS

- We manipulated hypolimnetic oxygen (O<sub>2</sub>) at the whole-ecosystem scale in a reservoir.
- Rapid O<sub>2</sub> shifts changed terminal electron acceptor budgets relative to a reference system.
- Our manipulations add insight into how redox pathways respond to varying O<sub>2</sub> availability.

## INTRODUCTION

Lakes and reservoir ecosystems globally are experiencing unprecedented changes in their dissolved oxygen (DO) concentrations due to land use and climate change, which has important implications for their biogeochemical cycling (Tranvik and others 2009; Marcé and others 2010; Jenny and others 2016). For example, increases in near-surface water (epilimnion) temperatures and eutrophication are depleting DO in the bottom waters (hypolimnion) of many lakes and reservoirs (Jenny and others 2016; Jokinen and others 2018; Vegas-Vilarrúbia and others 2018). Simultaneously, more frequent and powerful storms can increase mixing of oxic epilimnetic water across the thermocline into the hypolimnion, thereby temporarily increasing DO availability in the metalimnion and hypolimnion (for example, Jennings and others 2012; Klug and others 2012). These changes in DO availability can generate intermittent conditions of oxic, high-DO water and anoxic water with DO below 0.5 mg l<sup>-1</sup> in the metalimnion and hypolimnion.

As DO is expected to continue to change in lakes and reservoirs in the future (Jenny and others 2016; Vegas-Vilarrúbia and others 2018), it remains unclear to what extent alternate TEA pathways will change, which has implications for greenhouse gas dynamics and organic carbon burial (Figure 1). Because DO is the most energetically favorable terminal electron acceptor (TEA) in freshwater ecosystems, its availability controls the onset of anaerobic redox reactions (that is, alternate TEA pathways) for organic carbon mineralization (Stumm and Morgan 1996; Schlesinger 1997; Ta-

ble 1) and subsequent greenhouse gas production of dissolved carbon dioxide (CO<sub>2</sub>) and methane (CH<sub>4</sub>) (Stanley and others 2016). Alternate TEA pathways (for example, denitrification, manganese reduction, iron reduction, sulfate reduction, methanogenesis; see Table 1, Figure 1) mineralize organic carbon less efficiently than aerobic respiration (Schlesinger 1997; Hartnett and others 1998; Sobek and others 2009), and rates of organic carbon mineralization vary among alternate TEA pathways (Schlesinger 1997). Consequently, the rates of organic carbon burial and mineralization that produce dissolved carbon dioxide (CO<sub>2</sub>) and methane (CH<sub>4</sub>) in freshwaters are tightly coupled to DO availability (Figure 1; Bastviken and others 2004a). Lakes and reservoirs receive and process large quantities of organic carbon (Dean and Gorham 1998; Cole and others 2007; Downing and others 2008; Tranvik and others 2009; Knoll and others 2013; Mendonça and others 2017), can have high CO<sub>2</sub> and CH<sub>4</sub> production rates, and are important greenhouse gas sources to the atmosphere relative to their small surface area (Downing and others 2008; Tranvik and others 2009; Deemer and others 2016). Thus, it is critically important to understand how variability in the DO conditions in the water column will affect alternate TEA pathways and greenhouse gas production in lakes and reservoirs.

Although laboratory experiments of TEA pathways have improved our understanding of redox reactions in freshwater systems, expanding these experiments to the ecosystem scale may better represent how TEA pathways and CO<sub>2</sub> and CH<sub>4</sub> production may change in the future. Laboratory studies on TEA pathways in lakes and reservoirs have shown that alternate TEA pathways are initiated at low DO concentrations (Kelly and others 1988; Frindte and others 2015; Lau and others 2015, 2016; Corzo and others 2018). However, laboratory studies exclude many physical, chemical, and biological drivers that occur at the ecosystem scale (Carpenter 1996) and likely influence TEA pathways. For example, controlled laboratory experiments may mask the variability of TEA pathways occurring among different water column layers in a lake or reservoir, which could vary due to different DO conditions in the epilimnion, metalimnion, and hypolimnion. Some lakes and reservoirs exhibit metalimnetic DO minima during the stratified period (reviewed by McClure and others 2018), and it is unclear to what extent alternate TEA pathways occur in metalimnetic DO minima compared to anoxic hypolimnia. Ecosystem-scale manipulations are an established,

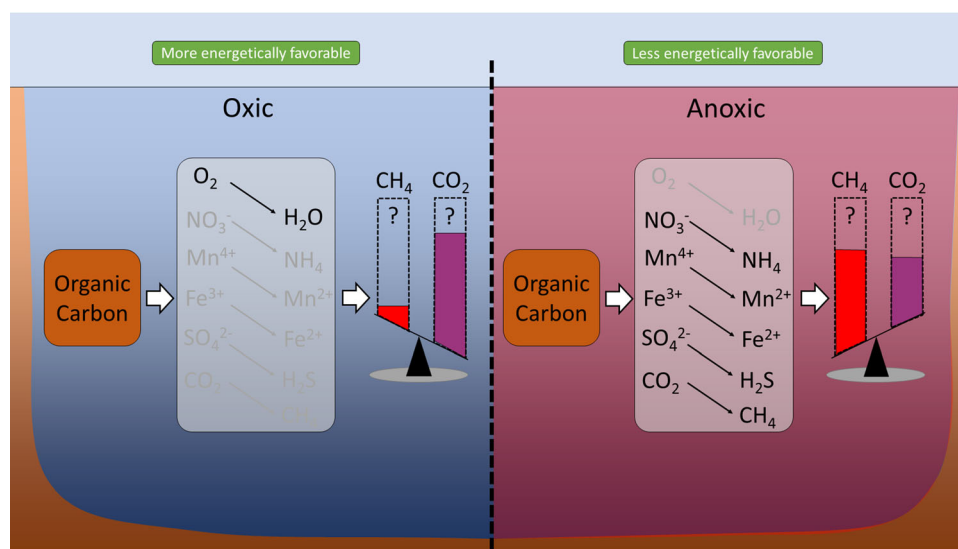


**Figure 1.** In oxic conditions (left panel), organic carbon is mineralized via aerobic respiration. In anoxic conditions (right panel), organic carbon is mineralized via alternate terminal electron acceptor (TEA) pathways. Decreasing oxygen availability will trigger organic carbon mineralization via alternate terminal electron acceptor pathways, which has the potential to control the relative production of CO<sub>2</sub> and CH<sub>4</sub> in the water column. In oxic conditions, CO<sub>2</sub> is expected to be the primary product of mineralization, whereas in anoxic conditions, both CO<sub>2</sub> and CH<sub>4</sub> will be produced depending on the dominant pathway, though their relative accumulation is unknown.

**Table 1.** Terminal Electron Acceptor Pathways of Organic Carbon Mineralization in Freshwater Ecosystems with Their Electron equivalents (following Schlesinger 1997 and Matthews and others 2008)

Pathway	Reduction Reaction	GHG product	Electron equivalents
Aerobic respiration	$O_2 + 4H^+ + 4e^- \leftrightarrow 2H_2O$	CO <sub>2</sub>	4
Denitrification	$NO_3^- + 6H^+ + 5e^- \leftrightarrow \frac{1}{2} N_2 + 3H_2O$	CO <sub>2</sub>	5
Manganese reduction	$MnO_2 + 4H^+ + 2e^- \leftrightarrow Mn^{2+} + 2H_2O$	CO <sub>2</sub>	2
Iron reduction	$Fe(OH)_3 + 3H^+ + e^- \leftrightarrow Fe^{2+} + 3H_2O$	CO <sub>2</sub>	1
Sulfate reduction	$SO_4^{2-} + 10H^+ + 8e^- \leftrightarrow H_2S + 4H_2O$	CO <sub>2</sub>	8
Methanogenesis	$CH_2O + 4H^+ + 4e^- \leftrightarrow CH_4 + H_2O$	CH <sub>4</sub>	4

Reactions are ordered by their thermodynamic favorability from most to least favorable. Aerobic respiration, denitrification, manganese reduction, iron reduction, and sulfate reduction all produce CO<sub>2</sub> as a result of organic carbon mineralization; methanogenesis produces CH<sub>4</sub>. We use e<sup>-</sup> to denote electrons in the reactions.

albeit challenging, approach for creating highly contrasting changes to help differentiate underlying causal mechanisms (Carpenter and others 1996; Schindler 1998), and can provide useful data for understanding how changing DO conditions alter TEA pathways and greenhouse gas dynamics.

A few ecosystem-scale investigations have monitored TEA pathways and CO<sub>2</sub> and CH<sub>4</sub> production in the water column of lakes and reservoirs (for example, Schafran and Driscoll 1987; Mattson and Likens 1992; Matthews and others 2008; Matzinger and others 2010). To the best of our knowledge, none of these studies monitored alternate TEA pathways and greenhouse gas production while manipulating DO at the ecosystem scale relative to a non-manipulated reference ecosystem. Matthews

and others (2008) and Matzinger and others (2010) evaluated TEA pathways in the hypolimnion of one lake but did not investigate other layers in the water column (that is, the epilimnion or metalimnion). Huttunen and others (2001) added oxic epilimnetic water to the anoxic hypolimnion of an ice-covered lake basin and showed that increasing hypolimnetic DO decreased CH<sub>4</sub> concentrations relative to a non-manipulated reference; however, they did not specifically examine the alternate TEA pathways. These previous ecosystem-scale experimental manipulations have provided robust assessments of changing oxygen conditions, suggesting that further oxygen experiments quantifying alternate TEA pathways and greenhouse gas

production can advance our understanding of how ecosystem functioning may change in the future.

Despite the need for ecosystem-scale experiments to examine how changing DO conditions affect alternate TEA pathways, evaluating these processes in a quantitative framework is challenging. One promising method for investigating experimentally manipulated TEA pathways is to calculate electron budgets (following Matthews and others 2008) by conducting mass balance calculations of depleting TEAs and accumulating TEPs over discrete time periods over the course of the monitoring period, and then comparing the relative proportion of the TEA pathways to the rate of CO<sub>2</sub> and CH<sub>4</sub> accumulation. Determining the relative contribution of TEA pathways to organic carbon mineralization and electron flow (Matthews and others 2008) under varying DO conditions among discrete layers in the water column can reveal patterns that would not be possible from measuring the concentrations of TEAs and TEPs alone.

We conducted an ecosystem-scale experiment adding supersaturated DO to the hypolimnion of a eutrophic reservoir with a hypolimnetic oxygenation (HOx) system (Gerling and others 2014). Our goal was to determine how contrasting DO conditions in different water column layers affected TEA pathways and subsequent accumulation of CO<sub>2</sub> and CH<sub>4</sub>. During the DO addition experiment, we measured the concentrations of (1) TEAs: dissolved oxygen (O<sub>2</sub>), nitrate (NO<sub>3</sub><sup>-</sup>), manganese IV (Mn<sup>4+</sup>), iron III (Fe<sup>3+</sup>), and sulfate (SO<sub>4</sub><sup>2-</sup>); (2) terminal electron products (TEPs): manganese II (Mn<sup>2+</sup>), iron II (Fe<sup>2+</sup>), carbon dioxide (CO<sub>2</sub>), and methane (CH<sub>4</sub>); and (3) redox potential (ORP) in the epilimnion, metalimnion, and hypolimnion in the experimental reservoir. We also monitored concentrations of the same TEAs and TEPs and redox potential in an upstream, non-oxygenated reservoir which served as a reference ecosystem. Finally, we calculated the relative contribution of the TEA pathways in both reservoirs using the electron budget method (described by Matthews and others 2008), and then related changes in TEA pathways to CO<sub>2</sub> and CH<sub>4</sub> accumulation rates.

## METHODS

### Site Description

The experimental reservoir in our study was Falling Creek Reservoir (FCR; Figure 2), a shallow ( $Z_{\max} = 9.3$  m,  $Z_{\text{mean}} = 4.0$  m), eutrophic reservoir located in Vinton, Virginia, USA (37.30°N, 79.84°W; Gerling and others 2016; Munger and

others 2016; Hamre and others 2017; McClure and others 2018). FCR is dimictic and thermally stratifies between April and October (McClure and others 2018). In the absence of oxygenation, FCR exhibits anoxia near the sediments and occasional algal blooms during the summer stratified period (Gerling and others 2014).

Beaverdam Reservoir (BVR, 37.31°N, 79.81°W; Figure 2) serves as a reference reservoir for FCR (Table 2) and has similar morphometry (during our study,  $Z_{\max} = 12$  m), water chemistry, and catchment land use history (Table 2) (Doubek and others 2018; Carey and others 2018a). BVR is located 3 km upstream and provides the primary inflow water that enters FCR via a 1.7 km-long stream (Gerling and others 2016; Munger and others 2019). BVR also experiences anoxia near the sediments and phytoplankton blooms (Hamre and others 2018). Both reservoirs, constructed in the late 1800s in catchments that have almost completely reforested after agricultural abandonment in the late 1930s, are owned and operated by the Western Virginia Water Authority (WVWA) as drinking water supplies (Gerling and others 2016). The bedrock geology underlying both reservoirs and the surrounding watershed is layered pyroxene granulite, a metamorphic formation rich in Fe and Mn-rich minerals (Virginia Division of Mineral Resources 2003).

### Hypolimnetic DO Manipulations

In 2012, the WVWA deployed a side-stream HOx in FCR to mitigate water quality problems (Gerling and others 2014; Munger and others 2016; McClure and others 2018). The HOx increases the DO concentrations in the hypolimnion without disrupting the reservoir's thermal stratification (Gerling and others 2014). The HOx system withdraws hypolimnetic water from 8.5 m depth and injects ~95% O<sub>2</sub> into the water in a contact chamber onshore, bringing it to supersaturated concentrations relative to the hypolimnion. The water is then pumped back to the reservoir at the same depth, inducing mixing of DO in the lower hypolimnion (Gerling and others 2014). For a detailed description of the HOx system, refer to Gerling and others (2014). As a consequence of HOx operation, a metalimnetic DO minimum can develop around the thermocline because mixing in the lower hypolimnion strengthens the thermal stability of the water column (Gerling and others 2014; McClure and others 2018). Settling particulates from the epilimnion will accumulate on the strong thermal gradient between the warm water

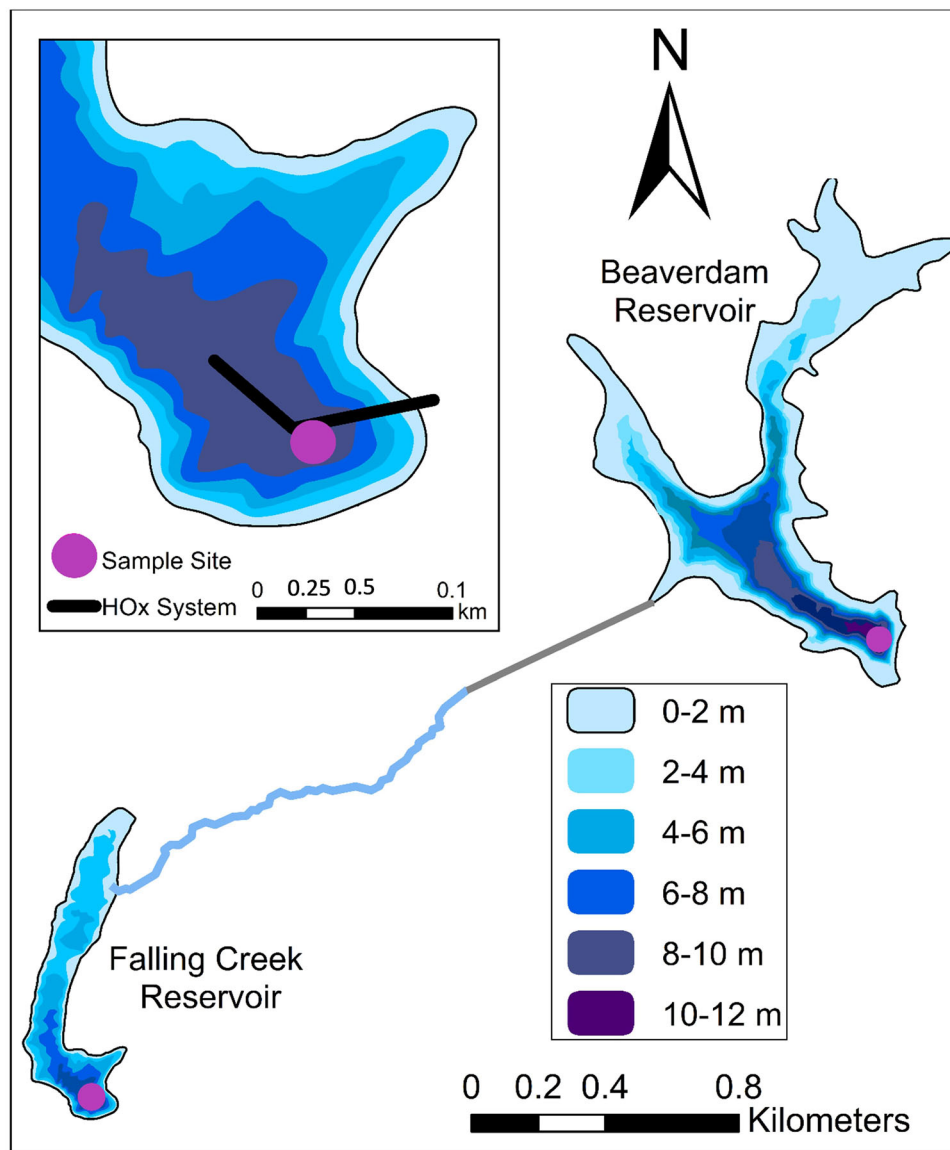


**Figure 2.** Bathymetric map of Falling Creek Reservoir (FCR), the experimental reservoir, and the reference Beaverdam Reservoir (BVR), Vinton, Virginia, USA. The red points show the sampling sites near the dams of both reservoirs. The inset shows a magnified view of the hypolimnetic oxygenation (HOx) system (denoted by the black line) that was used to manipulate dissolved oxygen concentrations throughout the hypolimnion of FCR.

in the epilimnion and cold, high-density water in the hypolimnion, intensifying the metalimnetic oxygen depletion via microbial respiration (Kreling and others 2017; McClure and others 2018).

For this study, the HOx was operated continuously from 18 April to 11 November 2016 to maintain high oxygen concentrations in the hypolimnion of FCR. The oxygen addition rate to the hypolimnion during this time ranged between 12.5 and 20 kg d<sup>-1</sup>, with a water flow rate during oxygenation periods of 227 L min<sup>-1</sup>. At this flow rate, the total hypolimnetic volume of FCR was circu-

lated through the HOx every 20–30 days (McClure and others 2018).

### Field Data Collection

We monitored the physical, chemical, and biological conditions in both reservoirs from 12 May to 12 October 2016. We collected depth profiles of temperature and DO twice weekly at the deepest site of FCR and weekly at the deepest site of BVR using a high-resolution (4 Hz sampling rate) SBE 19 plus Conductivity, Temperature, and Depth (CTD) profiler (Seabird Electronics, Bellevue, WA, USA). The

**Table 2.** Morphological and Water Quality Characteristics of the experimentally oxygenated Falling Creek Reservoir and reference Beaverdam Reservoir

Characteristics	Falling Creek Reservoir mean $\pm$ 1 S.D.	Beaverdam Reservoir mean $\pm$ 1 S.D.
Surface area (km <sup>2</sup> )	0.12	0.39
Maximum depth (m)	9.3	12.0
Mean depth (m)	4.0	6.0
Volume (m <sup>3</sup> )	$3.5 \times 10^5$	$1.3 \times 10^6$
Surface temperature (°C)	$23.8 \pm 3.5$	$24.6 \pm 3.3$
Chlorophyll <i>a</i> ( $\mu\text{g l}^{-1}$ )	$2.3 \pm 1.3$	$2.4 \pm 1.9$
Turbidity (NTU)	$2.0 \pm 0.9$	$1.8 \pm 0.6$

Mean temperature, conductivity, chlorophyll *a*, and turbidity were averaged from all measurements collected at 0.1 m depth at the deepest site of both reservoirs during the 2016 sampling period.

CTD collected depth profiles of temperature and DO at  $\leq 0.1$  m increments (Carey and others 2019a). We used temperature profiles from each CTD cast to calculate thermocline depths on the sampling days using LakeAnalyzer, a MATLAB program (Read and others 2011). We measured oxidation–reduction potential (ORP) using a YSI Pro-Quatro multi-parameter probe with an attached Pro Series 1002 ORP sensor (YSI Incorporated; Yellow Springs, OH, USA) that was calibrated with Zobell solution each sampling day (Carey and others 2018b). However, it is important to note that ORP should not be used to determine specific TEA pathways because ORP electrodes lack correlation between observed ORP values and Eh computed from coupled TEA pathways (Morris and Stumm 1967; Kehew 2000). Here, we chose to use ORP a guide to differentiate between oxidizing conditions (when DO is the dominant TEA) and reducing conditions (when alternate TEAs dominate).

We collected water samples for analysis of alternate TEAs ( $\text{NO}_3^-$ ,  $\text{Mn}^{4+}$ ,  $\text{Fe}^{3+}$ , and  $\text{SO}_4^{2-}$ ) and TEPs ( $\text{Mn}^{2+}$ ,  $\text{Fe}^{2+}$ , and dissolved  $\text{CO}_2$  and  $\text{CH}_4$ ) with a 4-l Van Dorn sampler (Wildlife Supply Co., Yulee, FL, USA) from three depths in FCR that represented the epilimnion (0.1 m), metalimnion (5.0 m), and hypolimnion (9.0 m). We collected water samples from BVR at similar depths (0.1, 6, and 11 m) to represent the three layers. For simplicity, we refer to  $\text{CO}_2$  as a TEP, even though we fully recognize that it can also serve as a TEA for hydrogenotrophic methanogenesis (Conrad 1989). Water for  $\text{NO}_3^-$ ,  $\text{SO}_4^{2-}$ , and  $\text{Fe}^{2+}$  samples was filtered through 0.7  $\mu\text{m}$  GF/F glass microfiber filters into HCl acid-washed sample bottles. Immediately after syringe-filtering in the field, we used 0.1 ml of the filtrate for  $\text{Fe}^{2+}$  analyses following Viollier and others (2000), and then froze the remaining water. Water samples for total Fe and Mn analysis were collected in new HDPE bottles; water samples for soluble Fe

and Mn analysis were filtered through 0.45  $\mu\text{m}$  nylon filters into new HDPE bottles. Both total and soluble metal samples were preserved using trace metal grade nitric acid to pH below 2 (Munger and others 2016). Dissolved  $\text{CH}_4$  and  $\text{CO}_2$  samples were collected by carefully filling two replicate 20-ml glass vials with unfiltered sample water. The vials were immediately capped with an airtight seal free of any headspace and kept on ice until analysis within 24 h (following McClure and others 2018).

### Laboratory Analyses

We followed standard procedures in the laboratory to quantify concentrations of alternate TEAs and TEPs (Carey and others 2019b, 2020). We measured  $\text{NO}_3^-$  using a Lachat flow injection analyzer (Lachat Instruments, Loveland, CO) following the Quik-Chem Method 10-115-10-1-B with a method detection limit of  $8.05 \times 10^{-5}$  mM. Samples were analyzed for Fe and Mn concentrations using an Inductively Coupled Plasma Optical Emission Spectrometer (ICP-OES, Spectro ARCOS) following EPA Method 200.7 (US EPA 1994). The method detection limits (MDL) for this method were  $7.2 \times 10^{-5}$  mM for Fe and  $1.8 \times 10^{-5}$  mM for Mn. We assumed that the total Fe concentration was the sum of  $\text{Fe}^{3+}$  and  $\text{Fe}^{2+}$  and subtracted the field-measured  $\text{Fe}^{2+}$  from the total Fe to calculate the concentration of  $\text{Fe}^{3+}$ , following Viollier and others (2000). Similarly, we assumed that total Mn concentration was the sum of  $\text{Mn}^{4+}$  and  $\text{Mn}^{2+}$  and that  $\text{Mn}^{2+}$  was represented by the soluble Mn concentration, following the work by Munger and others (2016, 2019) in the same reservoirs. We calculated  $\text{Mn}^{4+}$  as the difference between total Mn and  $\text{Mn}^{2+}$ .

$\text{SO}_4^{2-}$  was measured using ion chromatography (Dionex DX-120) following APHA Standard Method 3125-B with a MDL of  $6.04 \times 10^{-4}$  mM (APHA

1992). Dissolved  $\text{CO}_2$  and  $\text{CH}_4$  samples were analyzed using methods adapted from the U.S. EPA method RSKSOP-175 (Hudson 2004). Gas headspace was generated in the samples and analyzed on a flame ionization detector to calculate dissolved  $\text{CO}_2$  and  $\text{CH}_4$  (GC-FID; SRI Instruments, Torrance, CA) following McClure and others (2018) with an MDL of  $2.0 \times 10^{-6}$  mM and  $3.8 \times 10^{-3}$  mM, respectively.

## TEA Pathway Budgets

We evaluated the relative contribution of the TEA pathways to organic carbon mineralization between the metalimnion and hypolimnion over the monitoring period by calculating electron budgets following the method of Matthews and others (2008). We did not determine electron budgets for the epilimnion because it was consistently oxic throughout the period of thermal stratification in both reservoirs.

To calculate the electron budgets, we estimated depletion rates of TEAs and accumulation rates of TEPs, following Matthews and others (2008). First, we delineated time periods over which there was significant depletion of TEAs or accumulation of TEPs (Figures S1–S4). A detailed description of how we delineated the time periods of TEA depletion and TEP accumulation is provided in the Supporting Information (Text S1 and Figures S1:S4). Second, to quantify TEA and TEP rates in mass units ( $\text{mmol d}^{-1}$ ), we multiplied each rate by the mean volume (L) of the thermal layer in which it was measured. The mean volumes of the hypolimnion and metalimnion in FCR and BVR were determined using bathymetric data of the reservoirs (Gerling and others 2014; Carey and others 2018a). The upper and lower depths of the metalimnion were determined also using LakeAnalyzer (Read and others 2011), which calculated the metalimnetic boundaries from the CTD temperature profiles. We converted mass rates to fluxes of TEAs and TEPs ( $\text{mmol m}^{-2} \text{d}^{-1}$ ) by dividing the mass rates by the upper surface area of the represented layer. We adjusted the fluxes to account for any vertical diffusion between the epilimnion/metalimnion and metalimnion/hypolimnion in FCR and BVR following Matthews and others (2008); see Text S1 in the Supporting Information. To determine the TEA and TEP mass per unit area ( $\text{mmol m}^{-2}$ ), we multiplied the areal rates by the number of days within each discrete time period.

Third, we calculated the electron equivalents for each TEA pathway by converting mass fluxes according to electron equivalents in Table 1 ( $e^-$

$\text{eq m}^{-2}$ ). We used the same electron equivalents as Matthews and others (2008); however, it should be noted that the redox stoichiometry for some TEA pathways (for example, sulfate reduction and methanogenesis) can have varying electron equivalents (Stumm and Morgan 1996). Finally, we determined the relative contributions of each TEA pathway to the overall electron budget by dividing the contribution of each TEA pathway ( $\text{O}_2$ ,  $\text{NO}_3^-$ ,  $\text{SO}_4^{2-}$ ,  $\text{Mn}^{2+}$ ,  $\text{Fe}^{2+}$ , and  $\text{CH}_4$ ) by the sum of all of the TEA pathways. This was done separately for the metalimnion and hypolimnion in FCR and BVR. Examining the relative contributions of each TEA pathway among layers allowed us to determine how the TEA processes were affected by oxygenation of FCR in comparison with the reference (BVR) and how changes in TEA pathways affected the accumulation of  $\text{CO}_2$  and  $\text{CH}_4$ .

## RESULTS

Activation of the HOx system in FCR generated well-oxygenated conditions in the hypolimnion and anoxic conditions in the metalimnion, all while maintaining thermal stratification (Figure 3A, C). In contrast, BVR's hypolimnion became anoxic soon after the onset of thermal stratification in May and remained anoxic through the sampling period; the metalimnion became anoxic from 11 August to 27 September (Figure 3B, D). BVR's seasonal mean thermocline depth was similar to FCR's thermocline throughout the monitoring period ( $5.3 \pm 1.0$  m (1 S.D.) vs.  $5.8 \pm 1.0$  m, respectively). Both reservoirs' epilimnia remained oxic during the sampling period ( $\text{DO} \geq 6.3$  mg  $\text{l}^{-1}$ ). Fall turnover in FCR occurred on 9 October, while turnover had not occurred yet in BVR by the end of the monitoring period on 21 October (Figure 3A, B).

The well-oxygenated conditions in FCR's hypolimnion resulted in higher mean ORP values ( $210 \pm 38$  mV) in comparison with BVR's anoxic hypolimnion ( $-90 \pm 63$  mV; Figure 4). BVR's hypolimnion reached its lowest ORP value of  $-155$  mV on 23 August. We observed the lowest ORP in FCR's metalimnion on 2 September (0 mV), the same date as the lowest DO concentration (5 m, Figures 3C and 4A). This was the lowest ORP value observed among all of FCR's layers throughout the monitoring period. Conversely, BVR's metalimnion remained  $\geq 20$  mV during the monitoring period, despite becoming anoxic for 1 month (Figures 3D and 4B). FCR and BVR's seasonal mean epilimnetic ORP was similar during the sampling period ( $170 \pm 75$  mV and  $190 \pm 83$  mV, respectively).

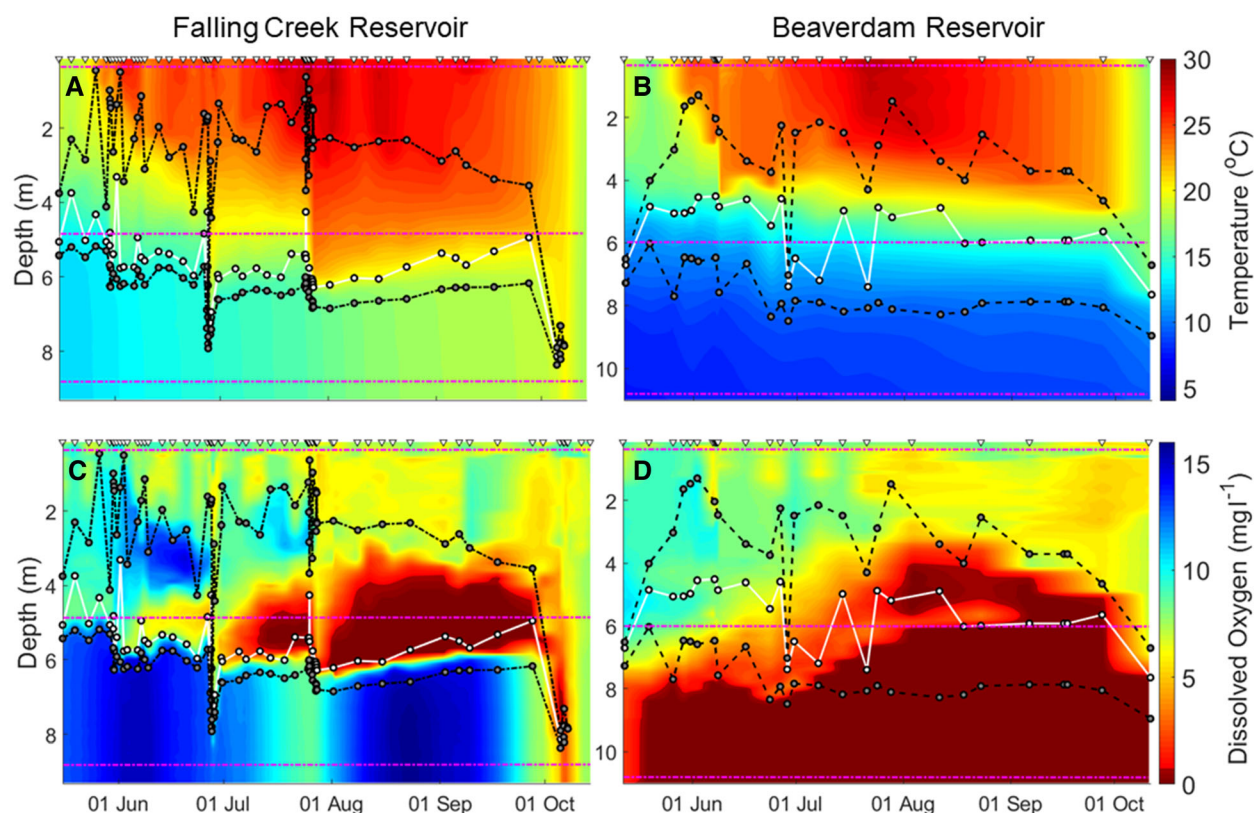


**Figure 3.** Temperature (**A, B**) and dissolved oxygen (**C, D**) heatmaps for Falling Creek (left column) and Beaverdam (right panel) Reservoirs. The horizontal pink lines show the epilimnetic, metalimnetic, and hypolimnetic depths sampled for oxidized terminal electron acceptors (TEAs) and reduced terminal electron products (TEPs). The gray dashed lines with circles represent the upper and lower depths of the metalimnion during the monitoring period and the solid white line with circles represents the thermocline. The color bar for the dissolved oxygen heatmaps (**C, D**) has a hard boundary at  $0.5 \text{ mg l}^{-1}$  (dark red) to indicate the boundary of anoxic and oxic conditions in the water column. The inverted white triangles at the top of the plots shows when temperature and dissolved oxygen profiles were collected; the intervening data were linearly interpolated.

### Seasonal TEA and TEP Patterns in FCR and BVR

Throughout the monitoring period, almost all TEAs and TEPs were detectable in both reservoirs in most layers, except  $\text{NO}_3^-$  (Figure 5). There were substantial seasonal differences in the TEA and TEP concentrations among depths in FCR and BVR over time, as described below.

In FCR's hypolimnion, DO remained above  $0.1 \text{ mM}$  ( $3.2 \text{ mg l}^{-1}$ ) for the entire monitoring period and reached its highest concentration at  $0.52 \text{ mM}$  ( $16 \text{ mg l}^{-1}$ ) on 26 August (Figure 5I). In addition to DO, other TEAs ( $\text{NO}_3^-$ ,  $\text{Fe}^{3+}$ , and  $\text{SO}_4^{2-}$ ) were also detectable in FCR's hypolimnion (Figure 5I). Despite the well-oxygenated conditions, we observed  $\text{Mn}^{2+}$  in the hypolimnion of FCR starting 19 June, which reached a peak concentration of  $0.02 \text{ mM}$  on 15 August before steadily decreasing until the end of the sampling period

(Figure 5J). There was not a concomitant increase in  $\text{Fe}^{2+}$  or  $\text{CH}_4$  during this period (Figure 5J), but there was a steady accumulation of  $\text{CO}_2$  in FCR's hypolimnion that occurred during 15 June–1 October that reached a peak concentration of  $0.6 \text{ mM}$  on 30 September (Figure 5J).

In contrast to FCR, BVR's hypolimnion was depleted of DO early in the monitoring period (Figure 5K). We also observed depletions of  $\text{Mn}^{4+}$  and  $\text{Fe}^{3+}$  and a corresponding increase in  $\text{Mn}^{2+}$  and  $\text{Fe}^{2+}$  throughout the monitoring period to a maximum of  $0.04$  and  $0.31 \text{ mM}$ , respectively (Figure 5L). Following the depletions in  $\text{Mn}^{4+}$  and  $\text{Fe}^{3+}$ , we observed depletions in  $\text{SO}_4^{2-}$  to below detection on 02 June (Figure 5K). Surprisingly, we also observed elevated  $\text{Fe}^{3+}$  concentrations up to  $0.048 \text{ mM}$  that occurred on 26 June, one full month after BVR's hypolimnion became anoxic; by late July,  $\text{Fe}^{3+}$  returned to low concentrations ( $< 0.002 \text{ mM}$ ) (Figure 5K).

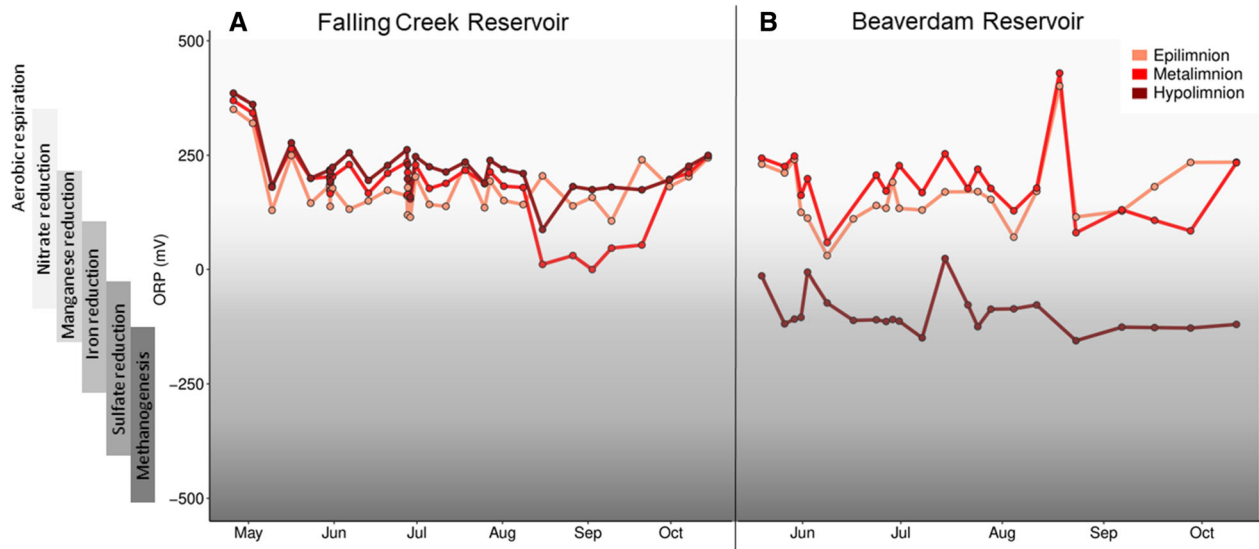


Figure 4. Oxidation–reduction potential (ORP) in millivolts (mV) during the monitoring period in the epilimnion (0.1 m), metalimnion (5.0 m and 6.0 m), and hypolimnion (9.0 m and 11.0 m) in Falling Creek (A) and Beaverdam (B) Reservoirs, respectively

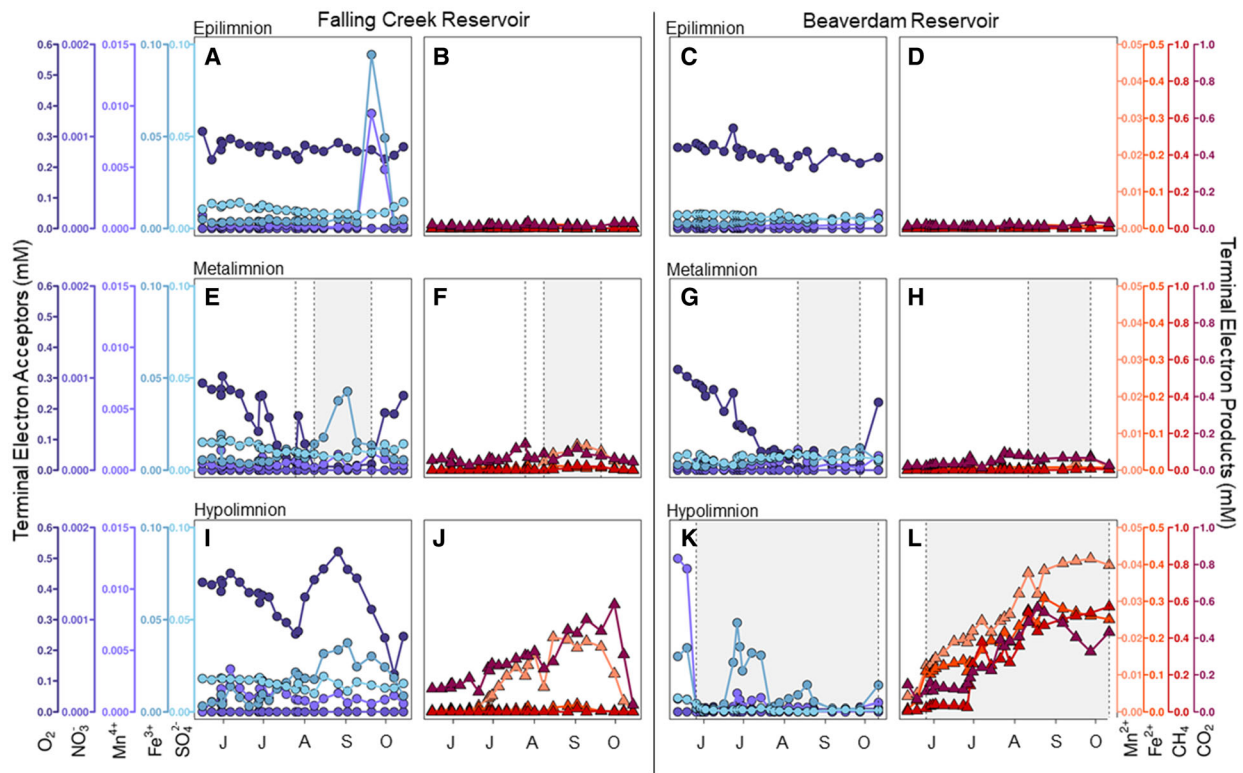


Figure 5. Concentrations of terminal electron acceptors (TEAs, circles) and terminal electron products (TEPs, triangles) from the epilimnion (0.1 m), metalimnion (5.0 m and 6.0 m), and hypolimnion (9.0 m and 11.0 m) depths in Falling Creek (A, B, E, F, I, J) and Beaverdam (C, D, G, H, K, L) Reservoirs, respectively. Shaded areas represent periods of anoxia ( $\text{DO} < 0.5 \text{ mg l}^{-1}$  or  $0.05 \text{ mM}$ ) that were observed at the corresponding depth. Axis colors correspond with the colors of the lines and points in the figure (see vertical labels, denoted by different colors for each TEA and TEP). All TEA and TEP concentrations are reported in mM for consistency.

The alternate TEA pathways in FCR and BVR's metalimnia varied despite both having low oxygen in August and September (Figure 5E–H). FCR's metalimnion became anoxic starting 8 August, which was followed by peak summer concentrations of  $\text{Mn}^{2+}$  and  $\text{CH}_4$  ( $6.9 \times 10^{-3}$  mM and 0.18 mM, respectively) that occurred on 2 September (Figure 5E, F). Although all other TEAs were at their lowest concentrations during this anoxic period, we observed that  $\text{Fe}^{3+}$  increased to its highest level of the sampling season (0.042 mM) on 2 September despite the strong reducing conditions. In contrast, BVR's metalimnion was anoxic from 11 August until 27 September (Figure 5G). Unlike the decline in TEAs ( $\text{DO}$  and  $\text{SO}_4^{2-}$ ) and slight increases in TEPs ( $\text{Mn}^{2+}$  and  $\text{CH}_4$ ) that we observed in FCR's metalimnion after the onset of anoxia, there were no substantial changes in TEA and TEP concentrations that occurred in BVR's metalimnion after it became anoxic (Figure 5G, H).

The epilimnia of both FCR and BVR remained oxic throughout the sampling period (Figure 3C, D), and as a result, there was no observable depletion of TEAs or increase in TEPs (Figure 5A–D). However, there was a substantial increase in  $\text{Mn}^{4+}$  and  $\text{Fe}^{3+}$  in FCR's epilimnion that occurred during 20–30 September, whereas no such increase was observed in BVR's epilimnion (Figure 5A). This 10-day period also corresponded with the last observed date of the metalimnetic DO minimum in FCR (Figure 3C).

### TEA Pathway Electron Budgets and $\text{CO}_2$ and $\text{CH}_4$ Accumulation Rates

In FCR's experimentally oxygenated hypolimnion, aerobic respiration contributed 84% of the total electron budget of organic carbon mineralization during the monitoring period, while the relative contribution from sulfate reduction was 9.3%, and all other TEA pathways contributed no more than 6.7% (Figure 6A, Table 3).  $\text{CO}_2$  dominated greenhouse gas accumulation in FCR's hypolimnion, with an accumulation rate of  $5.6 \text{ mmol m}^{-2} \text{ d}^{-1}$  versus  $0.04 \text{ mmol m}^{-2} \text{ d}^{-1}$  for  $\text{CH}_4$  (Figure 6B). Conversely, in BVR's anoxic hypolimnion, aerobic respiration only represented a small proportion of the total electron budget (7.4%), whereas the alternate TEA pathways, particularly methanogenesis, dominated organic carbon mineralization (Figure 6A, Table 3). In the hypolimnion of BVR,  $\text{CO}_2$  and  $\text{CH}_4$  accumulation rates were much more similar, at  $2.6 \text{ mmol m}^{-2} \text{ d}^{-1}$  and  $2.2 \text{ mmol m}^{-2} \text{ d}^{-1}$ , respectively (Figure 6B). Denitrification

played a negligible role in the electron budget of both reservoirs' hypolimnia (Table 3).

Comparison of the metalimnetic electron budgets between the manipulated and reference reservoir revealed important differences (Figure 6A, Table 3). In FCR's metalimnion, aerobic respiration contributed 84% of the electron budget, whereas methanogenesis contributed 8.0%; all other alternate TEA pathways contributed no more than 8.0%. We observed greater than tenfold higher accumulation rates of  $\text{CH}_4$  when the metalimnetic DO minimum formed in FCR from 1 August to 28 September (at  $0.3 \text{ mmol m}^{-2} \text{ d}^{-1}$ ) compared to FCR's hypolimnion (Figure 6B). The  $\text{CO}_2$  accumulation rate was  $0.5 \text{ mmol m}^{-2} \text{ d}^{-1}$  during this same time period. In BVR's metalimnion, aerobic respiration was the largest contributor to the overall electron budget (98%) and the alternate TEA pathways contributed no more than 2.0%. The  $\text{CH}_4$  accumulation rate during the anoxic period was similar to FCR's ( $0.2 \text{ mmol m}^{-2} \text{ d}^{-1}$ ), whereas the  $\text{CO}_2$  accumulation rate was slightly higher compared to FCR's metalimnion ( $0.9 \text{ mmol m}^{-2} \text{ d}^{-1}$ ) (Figure 6B, Table 3). As in the hypolimnetic electron budgets, denitrification played a negligible role in the two reservoirs' metalimnetic electron budgets.

## DISCUSSION

Our ecosystem-scale oxygenation additions altered TEA pathways in FCR. The HOx successfully manipulated DO conditions (Figure 3), which affected the redox potential and the progression of the alternate TEA pathways at the ecosystem scale (Figures 4, 5 and 6, Table 3). We found that increasing the DO in the hypolimnion of FCR inhibited the onset of alternate TEA pathways. In contrast, in the absence of oxygenation in BVR, TEA pathways followed a "classical" sequence following thermodynamic favorability (Table 1). Consequently, we observed much higher  $\text{CO}_2$  than  $\text{CH}_4$  accumulation under well-oxygenated conditions when alternate electron acceptor pathways were inactive, in comparison with more similar rates of  $\text{CO}_2$  and  $\text{CH}_4$  accumulation when alternate electron acceptor pathways were active in anoxic conditions (Figure 6B). Our ecosystem-scale manipulations of DO and comparison of a manipulated and reference freshwater reservoir add insight into how redox processes in lakes and reservoirs may change in the future as the availability of DO in the water column becomes more variable.

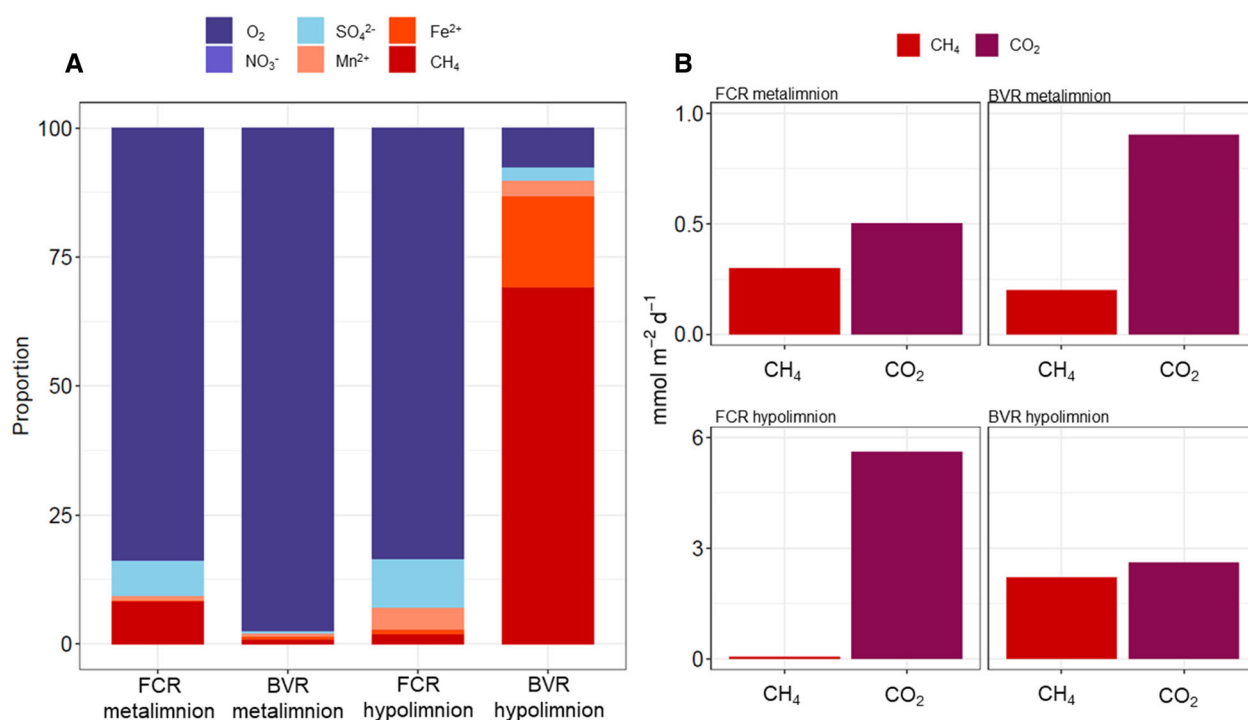


**Figure 6.** Bar chart (A) of the relative proportion of the total electron budget contributed by aerobic respiration, denitrification, sulfate reduction, manganese reduction, iron reduction, and methanogenesis in the metalimnion and hypolimnion in Falling Creek and Beaverdam Reservoirs during the monitoring period in 2016. The standard error associated with the relative proportions of the total electron budgets can be found in Table 3. CH<sub>4</sub> and CO<sub>2</sub> accumulation rates (B) were much more similar in the anoxic FCR metalimnion and BVR hypolimnion than in the oxic FCR hypolimnion and BVR metalimnion, where CO<sub>2</sub> accumulation dominated. Similar to Figure 5, blue-colored bars represent TEA depletion and the red-colored bars represent TEP accumulation. Note the y-axes for the metalimnetic and hypolimnetic layers vary.

**Table 3.** Comparison of the Metalimnetic and Hypolimnetic Electron Equivalent Budgets ( $\pm 1$  S.E.) and CO<sub>2</sub> and CH<sub>4</sub> Accumulation Rates (mmol m<sup>-2</sup> d<sup>-1</sup>) During the 2016 Monitoring Period

Water column layer	O <sub>2</sub> (%)	NO <sub>3</sub> <sup>-</sup> (%)	Mn <sup>2+</sup> (%)	Fe <sup>2+</sup> (%)	SO <sub>4</sub> <sup>2-</sup> (%)	CH <sub>4</sub> (%)	CO <sub>2</sub> (mmol m <sup>-2</sup> d <sup>-1</sup> )	CH <sub>4</sub> (mmol m <sup>-2</sup> d <sup>-1</sup> )
FCR metalimnion	84 $\pm$ 0.86	0	0.8 $\pm$ 0.20	0.2 $\pm$ 0.09	7.0 $\pm$ 0.14	8.0 $\pm$ 1.33	0.5	0.3
BVR metalimnion	96 $\pm$ 0.07	0	0.2 $\pm$ 0.16	0.3 $\pm$ 0.06	0.7 $\pm$ 0.64	0.8 $\pm$ 0.57	0.9	0.2
FCR hypolimnion	84 $\pm$ 0.28	0	4.0 $\pm$ 0.12	1.0 $\pm$ 0.32	9.3 $\pm$ 0.14	1.7 $\pm$ 1.26	5.6	0.04
BVR hypolimnion	7.4 $\pm$ 1.14	0	3.0 $\pm$ 0.09	18 $\pm$ 0.62	2.6 $\pm$ 0.12	69 $\pm$ 1.18	2.6	2.2

## Two Contrasting Hypolimnia

The hypolimnetic DO additions in FCR promoted aerobic respiration as the dominant organic carbon mineralization pathway in FCR's hypolimnion throughout the monitoring period (Figure 6A, Table 3). Alternate TEA pathways, including man-

ganese and iron reduction, also occurred in FCR's hypolimnion between July and September during the well-oxygenated conditions. The iron and manganese reduction likely occurred within the anoxic sediments, where Mn<sup>4+</sup> and Fe<sup>3+</sup> hydroxides are plentiful (Krueger and others 2020). Under

anoxic conditions in the sediment porewater, these metal hydroxides are reductively dissolved, releasing  $\text{Mn}^{2+}$  and  $\text{Fe}^{2+}$  that can diffuse into the water column even if it is well-oxygenated (Bryant and others 2011; Munger and others 2016; Krueger and others 2020). Due to a rapid oxidation rate,  $\text{Fe}^{2+}$  was likely oxidized as soon as it reached the oxygenated hypolimnetic water (Munger and others 2016).  $\text{Mn}^{2+}$ , however, accumulated in the well-oxygenated hypolimnion (Figure 5I). This is likely because Mn oxidizes more slowly than Fe, especially under the low pH conditions ( $\sim 5.9$ ) in the hypolimnion of FCR (Munger and others 2016; Carey and others 2018b; Krueger and others 2020). We compared our observed  $\text{Mn}^{2+}$  fluxes in FCR's hypolimnion to Krueger and others (2020) during periods when DO was added via HOx. Krueger and others (2020) reported soluble Mn fluxes up to  $0.3 \text{ mmol m}^{-2} \text{ d}^{-1}$  during oxygenation that occurred between 24 April and 14 July 2018 ( $\sim 2.5$  months). We observed  $\text{Mn}^{2+}$  fluxes in this study up to  $0.4 \text{ mmol m}^{-2} \text{ d}^{-1}$  during oxygenation between 18 July and 24 August in 2016. The similar  $\text{Mn}^{2+}$  fluxes in both studies highlight how Mn can consistently be released into the water column from the sediments during well-oxygenated conditions and that much of the TEP accumulation observed in the hypolimnion results from sediment diffusion.

Compared to FCR, a classic alternate TEA pathway sequence was observed in BVR's hypolimnion after the hypolimnion became anoxic (Table 1, Figure 5). Depletion of DO was followed rapidly by depletion of  $\text{Mn}^{4+}$  and  $\text{Fe}^{3+}$ , and then by a slightly delayed depletion of  $\text{SO}_4^{2-}$ . Concomitant with TEA depletions was an increase in TEP concentrations (Figure 5I) and low ORP values that persisted throughout the monitoring period (Figure 4B). Surprisingly, we also observed elevated concentrations of  $\text{Fe}^{3+}$  and  $\text{Mn}^{4+}$  for four consecutive weeks when the hypolimnion was anoxic (Figure 5K), although it should be noted that these  $\text{Fe}^{3+}$  and  $\text{Mn}^{4+}$  concentrations were considerably lower ( $3.5\times$  and  $12\times$ , respectively) than  $\text{Fe}^{2+}$  and  $\text{Mn}^{2+}$  concentrations measured during this same time period. The presence of  $\text{Fe}^{3+}$  and  $\text{Mn}^{4+}$  in the anoxic water column suggests that oxidation coupled with the reduction of another electron acceptor occurred under anoxic conditions.

The 4-week increase in  $\text{Fe}^{3+}$  and  $\text{Mn}^{4+}$  in BVR's anoxic hypolimnion provides the opportunity to disentangle the complexities of alternate TEA pathways at the ecosystem scale. Previous studies have shown that the reduction of alternate TEAs (for example,  $\text{Mn}^{4+}$ ) can be coupled with  $\text{Fe}^{2+}$

oxidation (Picardal 2012). This process was invoked by Krueger and others (2020) to explain concomitant increases in  $\text{Fe}^{3+}$  and  $\text{Mn}^{2+}$  in benthic flux chamber experiments conducted at FCR. This process, coupled with evidence for light-driven anaerobic oxidation of  $\text{Mn}^{2+}$  (Daye and others 2019), could explain the observed increases in both  $\text{Fe}^{3+}$  and  $\text{Mn}^{4+}$  during the same time period (12 June to 15 July), as these increases occurred at the time of highest water clarity observed in BVR in 2016 (Secchi depth = 3.5 m; Carey and others 2019c). It is possible that light may have been able to penetrate into anoxic layers of the water column and activate  $\text{Mn}^{2+}$  oxidation to regenerate  $\text{Mn}^{4+}$ , which could then be coupled to  $\text{Fe}^{2+}$  oxidation. Although the light-driven oxidation hypothesis remains to be tested, in situ observations such as these can help catalyze future studies that link the recent research on "new" redox pathways observed in controlled laboratory studies with ecosystem-scale observations.

## Two Contrasting Metalimnia

We observed different TEA pathways in the metalimnetic DO minima that formed as a result of the hypolimnetic DO manipulations in FCR, and naturally in BVR (Figures 5 and 6, Table 3). After DO was depleted in FCR's metalimnion, increases in  $\text{Mn}^{2+}$  and decreases in  $\text{SO}_4^{2-}$  were observed, concomitant with increases in  $\text{CH}_4$ . Overall, after aerobic respiration, methanogenesis accounted for the largest relative proportion of the electron budget in this layer (Figure 6A, Table 3). The transition from aerobic respiration to methanogenesis was rapid (Figure 5, Figure S1), suggesting that the  $\text{CH}_4$  measured in the metalimnion may have been produced in the sediments or hypolimnion and diffused upward (Rudd and Hamilton 1978; Bastviken and others 2004b; Peeters and others 2019) or entered laterally from the littoral zone or upstream (DelSontro and others 2018). The lack of other alternate TEA pathways (for example,  $\text{Mn}^{4+}$  reduction,  $\text{Fe}^{3+}$  reduction) observed in the metalimnetic DO minimum could have resulted from our sampling depth profile intervals. We used 5 m to represent the metalimnetic DO minimum despite observing anoxia at depths as deep as 6.2 m and as shallow as 3.8 m (Figure 3C). Thus, investigating how alternate TEA pathways change across depth within metalimnetic DO minima may provide further insight into how these low-DO zones affect lakes and reservoir biogeochemical cycling. These results highlight that the thicknesses of the epilimnion, metalimnion, and hypolimnion can

change over the season, underscoring the need for detailed spatial and temporal sampling.

BVR's metalimnion became anoxic within nine days of FCR's metalimnion also becoming anoxic (Figure 3). However, the contribution of alternate TEA pathways to the overall electron budget was considerably less in BVR than in FCR (Figure 6A, Table 3). After DO was depleted on 11 August, manganese reduction, sulfate reduction, and methanogenesis were active, resulting in the production of some CH<sub>4</sub> but less overall in comparison with FCR's metalimnion (Figure 6B, Table 3). The contrasting patterns between FCR's and BVR's metalimnia underscore that the progression of TEA pathways, and as a result, the relative contribution of TEA pathways to organic carbon mineralization, are strongly influenced by the timing of anoxia onset. For example, in FCR's metalimnion, DO was depleted by 2 August, allowing for manganese reduction, sulfate reduction, and methanogenesis to occur before fall turnover on 14 October. In contrast, DO in BVR's metalimnion was not fully depleted until 11 August; some Mn reduction was observed after anoxic conditions developed, but fall turnover occurred in BVR before other TEA pathways were activated.

Understanding how metalimnetic redox pathways are altered by global change has important implications for lake and reservoir biogeochemistry. Kreling and others (2017) showed how metalimnetic DO minima are fueled by downward fluxes of organic matter (for example, surface cyanobacteria blooms), which are anticipated to increase in the future (Carey and others 2012). The potential increase in metalimnetic DO minimum zones in lakes and reservoirs will influence biogeochemical processes, such as nitrogen loss (De Brabandere and others 2014). Furthermore, these low DO zones can mix with the epilimnion during storms, potentially degassing CO<sub>2</sub> and CH<sub>4</sub> accumulated within the metalimnion (McClure and others 2018). In contrast to the metalimnetic DO minima observed in our reservoirs, some waterbodies have also experienced an increased occurrence of metalimnetic DO maxima as a result of both physical and biological processes (Wilkinson and others 2015). Both of these metalimnetic phenomena (DO minima and DO maxima) create sharp redox boundaries with the overlying epilimnion and the underlying hypolimnion. As DO dynamics in lakes and reservoirs change in the future, results of DO manipulation experiments at the ecosystem scale, such as the one described in this study, are critically important for exploring how ecosystem processes will respond.

## Implications of Altered TEA Pathways for Greenhouse Gas Accumulation

Due to the high rates of aerobic respiration as a result of oxygenation, we observed up to 2.1-fold higher CO<sub>2</sub> accumulation rates in FCR's hypolimnion than in BVR's anoxic hypolimnion (Figure 6B, Table 3). A previous modeling study in FCR suggested that oxygenation may mineralize large quantities of sediment organic carbon into CO<sub>2</sub>, which will accumulate in the hypolimnion until turnover, when it can be emitted to the atmosphere (Carey and others 2018c). This earlier work supports our calculations that 84% of the total electron budget of organic carbon mineralization in FCR was attributable to aerobic respiration, resulting in rates up to 5.6 mmol m<sup>-2</sup> d<sup>-1</sup> of CO<sub>2</sub> accumulation prior to turnover.

In contrast, BVR's hypolimnion had minimal aerobic respiration (7.4%) and was dominated by methanogenesis (69%), resulting in CH<sub>4</sub> accumulation rates 55 times higher than in FCR's oxic hypolimnion (Figure 6B, Table 3). Although FCR and BVR are both considered eutrophic, agricultural practices in the watershed were curtailed about 90 years prior to this study (Gerling and others 2016). Older reservoirs, such as BVR and FCR, are known to both accumulate and emit less CH<sub>4</sub> compared to newly inundated reservoirs (Barros and others 2011; Prairie and others 2018).

In addition to CH<sub>4</sub>, CO<sub>2</sub> also accumulated at relatively high rates in BVR's anoxic hypolimnion, although at lower rates than in FCR's oxic hypolimnion (Figure 6B, Table 3). The accumulation of CO<sub>2</sub> in BVR's hypolimnion likely was due to organic carbon mineralization from the alternate TEA pathways under anoxic conditions prior to methanogenesis (that is, denitrification, manganese reduction, iron reduction, sulfate reduction; Table 1, Schlesinger 1997), and acetoclastic methanogenesis (Conrad 1989). Additionally, anaerobic oxidation of CH<sub>4</sub> is ubiquitous in freshwater hypolimnia (Sivan and others 2011; Bles and others 2014; Oswald and others 2015; Deutzmann 2020) and may have also contributed to the CO<sub>2</sub> accumulation in BVR's anoxic hypolimnion. Our results support observations by Huttunen and others (2001), who measured similar production rates of CO<sub>2</sub> and CH<sub>4</sub> in the hypolimnion of an anoxic ice-covered lake basin (Figure 6B, Table 3).

The results of our oxygen manipulations demonstrated that addition of DO alters TEA pathways, thereby also altering the production of greenhouse gases. However, we also found that the total greenhouse gas (CH<sub>4</sub> + CO<sub>2</sub>) accumulation to

be similar between the hypolimnia of FCR and BVR (Figure 5). This result suggests that alternating DO conditions in the water column can change the predominant greenhouse gas that is present but may not affect the total accumulation of carbon-based greenhouse gases in the water column. Additionally, the final fate of the CH<sub>4</sub> and CO<sub>2</sub> that accumulated within the metalimnion and hypolimnion remains unknown and warrants investigation. In particular, it is unclear what proportion of the dissolved CH<sub>4</sub> that accumulated in BVR's hypolimnion and FCR's metalimnion was emitted to the atmosphere at fall turnover versus oxidized in the water column (Mayr and others 2020). Similarly, the fate of the CO<sub>2</sub> that accumulated in FCR's hypolimnion due to oxygenation is also unknown. Additional ecosystem-scale oxygenation experiments quantifying the production and fate of greenhouse gases will improve our understanding of lake and reservoir TEA pathway budgets and the subsequent diffusive emissions.

### Challenges with Ecosystem-Scale Studies of TEA Pathways

Finally, there are limitations to examining TEA pathways using our ecosystem-scale experimental approach. For example, we were only able to evaluate the TEA pathways at one site per reservoir and did not directly quantify the horizontal transport of our TEA and TEP constituents from upstream sediments, which can be a substantial source of TEAs into the water column (Lau and others 2016; Deemer and Harrison 2019). Horizontal transport of CH<sub>4</sub> from methanogenesis occurring in upstream anoxic sediments may be an important driver of the accumulation of CH<sub>4</sub> in the metalimnetic DO minimum of FCR (Rudd and Hamilton 1978; DelSontro and others 2018), but we were unable to quantify that flux in this study. Measurement of  $\delta^{13}\text{C}-\text{CH}_4$  concentrations in the two reservoirs in future work would help determine if the CH<sub>4</sub> that accumulated at the deepest sites was produced in the sediments or water column following DelSontro and others (2018).

Accounting for different methanogenesis pathways is important when investigating the relative contribution of methanogenesis to electron budgets. Here, we followed the precedent of Matthews and others (2008) and assumed that the dominant pathway of methanogenesis is acetoclastic methanogenesis, with 4  $e^-$  in the electron budget. If hydrogenotrophic methanogenesis (Galand and others 2005) dominated, the relative contribution of methanogenesis to the electron budget would be

greater because of the higher electron equivalents from the reaction (8  $e^-$ ). For future work, differentiating between acetoclastic and hydrogenotrophic methanogenesis by measuring  $\delta^{13}\text{C}-\text{CH}_4$  concentrations (Gehring and others 2015) can improve electron budgets by informing when each reaction is contributing most to CH<sub>4</sub> production.

Another limitation of this study is the assignment of specific TEA pathways at specific time periods using TEA and TEP concentrations. Studies by Chapelle and others (1995) have shown that dissolved H<sub>2</sub> concentrations in the water column are a better indicator of the dominant alternate TEA pathway than measuring TEA and TEP concentrations. At best, we are limited to interpreting which TEA pathway dominated using weekly measurements, which may not have captured rapid biogeochemical reactions (for example, McClain and others 2003). However, throughout the monitoring period, our weekly sampling rates were still able to successfully capture changes in the overall TEA dynamics from the hypolimnetic DO manipulations in FCR.

### CONCLUSIONS

Lake and reservoir ecosystems globally are experiencing unprecedented changes in their DO concentrations due to land use and climate change (Jenny and others 2016). Our DO manipulations are one of the few empirical ecosystem-scale studies (to the best of our knowledge) that disentangle how DO availability in lakes and reservoirs affects TEA pathways. TEA pathways are challenging to quantify in situ yet have major effects governing biogeochemical reactions occurring in the water column (Weathers and Stayer 2013), and our study provides insight into future TEA dynamics in freshwater ecosystems with variable DO. For example, lakes and reservoirs experiencing longer durations of hypolimnetic anoxia will likely exhibit alternate TEA pathways in the water column, producing both CO<sub>2</sub> and CH<sub>4</sub>. Conversely, waterbodies that experience increasing extreme storm events and rapid re-oxygenation of the water column will likely exhibit only aerobic respiration, potentially producing substantial quantities of CO<sub>2</sub> over relatively short time periods. Altogether, our ecosystem-scale DO manipulations show that TEA pathways will rapidly respond to changing DO conditions and consequently alter CO<sub>2</sub> and CH<sub>4</sub> accumulation rates. Thus, as increased anoxic bottom waters and more frequent and powerful storms simultaneously change the DO dynamics of freshwater lakes and reservoirs, there will likely be

concomitant changes in the redox reactions in the water column that control organic carbon mineralization and greenhouse gas accumulation.

## ACKNOWLEDGEMENTS

We thank the WVWA for access to field sites and their long-term support of our work. We thank Bobbie Neiderlehner for her crucial help in the analytical chemistry laboratory and the Reservoir Group laboratory members who provided useful feedback in summer 2016, particularly Jonathan Doubek, Zachary Munger, Charlotte Harrell, and Kylie Campbell. Paul Hanson, Erin Hotchkiss, members of the Carey Lab, and GLEON colleagues provided helpful feedback throughout the development of the manuscript. This work was financially supported by NSF DEB-1753639, CNS-1737424, and DBI-1933016. Supporting figures and text for the manuscript can be found in the Supporting Information.

## DATA AVAILABILITY

All datasets analyzed in this manuscript are cited therein and available in the Environmental Data Initiative (EDI) repository. The DOIs for the datasets are: <https://doi.org/10.6073/pasta/6a382debf76aa74a56232ec87aabccd>, <https://doi.org/10.6073/pasta/8f19c5d19d816857e55077ba20570265>, <https://doi.org/10.6073/pasta/8f19c5d19d816857e55077ba20570265>, <https://doi.org/10.6073/pasta/e9b8ee83bc7fad6dcd439a41ad80a3c>, and <https://doi.org/10.6073/pasta/13c628ee3dc68d709c3a56cb61b9c747h>.

## Compliance with Ethical Standards

**Conflict of interest** The authors declare that they have no conflict of interest.

## REFERENCES

- APHA. 1992. Standard methods for the examination of water and wastewater. Washington DC: American Public Health Association, American Water Works Association, Water Environment Federation.
- Barros N, Cole JJ, Tranvik LJ, Prairie YT, Bastviken D, Huszar VL, del Giorgio P, Roland F. 2011. Carbon emission from hydroelectric reservoirs linked to reservoir age and latitude. *Nat Geosci* 4:593–6.
- Bastviken D, Persson L, Odham G, Tranvik LJ. 2004a. Degradation of dissolved organic matter in oxic and anoxic lake water. *Limnol Oceanogr* 49:109–16.
- Bastviken D, Cole J, Pace M, Tranvik L. 2004b. Methane emissions from lakes: dependence of lake characteristics, two regional assessments, and a global estimate. *Global Biogeochem Cycles* 18:GB4009.
- Blees J, Niemann H, Wenk CB, Zopfi J, Schubert CJ, Kirf MK, Veronesi ML, Hitz C, Lehmann MF. 2014. Micro-aerobic bacterial methane oxidation in the chemocline and anoxic water column of deep south-Alpine Lake Lugano (Switzerland). *Limnol Oceanogr* 59:311–24.
- Bryant LD, Hsu-Kim H, Gantzer PA, Little JC. 2011. Solving the problem at the source: controlling Mn release at the sediment–water interface via hypolimnetic oxygenation. *Water Res* 45:6381–92.
- Carey CC, Ibelings BW, Hoffmann EP, Hamilton DP, Brookes JD. 2012. Eco-physiological adaptations that favour freshwater cyanobacteria in a changing climate. *Water Res* 46:1394–407.
- Carey CC, McClure RP, Doubek JP, Lofton ME, Ward NK, Scott DT. 2018a. *Chaoborus* spp. transport CH<sub>4</sub> from the sediments to the surface waters of a eutrophic reservoir, but their contribution to water column CH<sub>4</sub> concentrations and diffusive efflux is minor. *Environ Sci Tech* 52:1165–73.
- Carey CC, Gerling AB, Doubek JP, Hamre KD, McClure RP, Lofton ME, Farrell KJ. 2018b. Secchi depth data and discrete depth profiles of photosynthetically active radiation, temperature, dissolved oxygen, and pH for Beaverdam Reservoir, Carvins Cove Reservoir, Falling Creek Reservoir, Gatewood Reservoir, and Spring Hollow Reservoir in southwestern Virginia, USA 2013–2017. Environmental Data Initiative repository . <https://doi.org/10.6073/pasta/6a382debf76aa74a56232ec87aabccd>.
- Carey CC, Doubek JP, McClure RP, Hanson PC. 2018c. Oxygen dynamics control the burial of organic carbon in a eutrophic reservoir. *Limnol Oceanogr Lett* 3(3):293–301.
- Carey CC, McClure RP, Gerling AB, Doubek JP, Chen S, Lofton ME, Hamre KD. 2019a. Time series of high-frequency profiles of depth, temperature, dissolved oxygen, conductivity, specific conductivity, chlorophyll a, turbidity, pH, oxidation–reduction potential, photosynthetic active radiation, and descent rate for Beaverdam Reservoir, Carvins Cove Reservoir, Falling Creek Reservoir, Gatewood Reservoir, and Spring Hollow Reservoir in Southwestern Virginia, USA 2013–2018. Environmental Data Initiative Repository . <https://doi.org/10.6073/pasta/8f19c5d19d816857e55077ba20570265>.
- Carey CC, Lofton ME, Gerling AB, McClure RP, Doubek JP, Niederlehner BR, Farrell KJ. 2019b. Water chemistry time series for Beaverdam Reservoir, Carvins Cove Reservoir, Falling Creek Reservoir, Gatewood Reservoir, and Spring Hollow Reservoir in southwestern Virginia, USA 2013–2018. Environmental Data Initiative Repository . <https://doi.org/10.6073/pasta/08a8d297003c8e8593f888980f52bbcf>.
- Carey CC, Gerling AB, Doubek JP, Hamre KD, McClure RP, Lofton ME, Farrell KJ, Wander HL. 2019c. Secchi depth data and discrete depth profiles of photosynthetically active radiation, temperature, dissolved oxygen, and pH for Beaverdam Reservoir, Carvins Cove Reservoir, Falling Creek Reservoir, Gatewood Reservoir, and Spring Hollow Reservoir in southwestern Virginia, USA 2013–2018 ver 7. Environmental Data Initiative . <https://doi.org/10.6073/pasta/e9b8ee83bc7fad6dcd439a41ad80a3c>.
- Carey CC, McClure RP, Schreiber ME, Lofton ME, Krueger KM. 2020. Time series of iron (II) and sulfate concentrations for Beaverdam and Falling Creek Reservoirs in southwestern Virginia, USA during 2016 ver 0. Environmental Data Initiative . <https://doi.org/10.6073/pasta/13c628ee3dc68d709c3a56cb61b9c747>.

- Carpenter SR. 1996. Microcosm experiments have limited relevance for community and ecosystem ecology. *Ecology* 77:677–80.
- Carpenter SR, Kitchell JF, Cottingham KL, Schindler DE, Christensen DL, Post DM, Voichick N. 1996. Chlorophyll variability, nutrient input, and grazing: evidence from whole-lake experiments. *Ecology* 77:725–35.
- Chapelle FH, McMahon PB, Dubrovsky NM, Fujii RF, Oaksford ET, Vroblesky DA. 1995. Deducing the distribution of terminal electron-accepting processes in hydrologically diverse groundwater systems. *Water Resour Res* 31:359–71.
- Cole JJ, Prairie YT, Caraco NF, McDowell WH, Tranvik LJ, Striegl RG, Duarte CM, Kortelainen P, Downing JA, Middelburg JJ, Melack JM. 2007. Plumbing the global carbon cycle: integrating inland waters into the terrestrial carbon budget. *Ecosystems* 10:172–85.
- Conrad R. 1989. Control of methane production in terrestrial ecosystems. In: Andreae MO, Schimel DS, Eds. Exchange of trace gases between terrestrial ecosystems and the atmosphere. Dahlem Konferenzen. Chichester: Wiley. p 39–58.
- Corzo A, Jiménez-Arias JL, Torres E, García-Robledo E, Lara M, Papaspyrou S. 2018. Biogeochemical changes at the sediment–water interface during redox transitions in an acidic reservoir: exchange of protons, acidity and electron donors and acceptors. *Biogeochemistry* 139:241–60.
- Daye M, Klepac-Ceraj V, Pajusalu M, Rowland S, Farrell-Sherman A, Beukes N, Bosak T. 2019. Light-driven anaerobic microbial oxidation of manganese. *Nature* 576:311–14.
- Dean WE, Gorham E. 1998. Magnitude and significance of carbon burial in lakes, reservoirs, and peatlands. *Geology* 26:535–8.
- De Brabandere L, Canfield DE, Dalsgaard T, Friederich GE, Revsbech NP, Ulloa O, Thamdrup B. 2014. Vertical partitioning of nitrogen-loss processes across the oxic–anoxic interface of an oceanic oxygen minimum zone. *Environ Micro* 16:3041–54.
- Deemer BR, Harrison JA, Li S, Beaulieu JJ, DelSontro T, Barros N, Bezerra-Neto JF, Powers SM, dos Santos MA, Vonk JA. 2016. Greenhouse gas emissions from reservoir water surfaces: a new global synthesis. *BioScience* 66:949–64.
- Deemer BR, Harrison JA. 2019. Summer redox dynamics in a eutrophic reservoir and sensitivity to a summer’s end draw-down event. *Ecosystems* 22:1618–32.
- DelSontro T, del Giorgio PA, Prairie YT. 2018. No longer a paradox: the interaction between physical transport and biological processes explains the spatial distribution of surface water methane within and across lakes. *Ecosystems* 21:1073–87.
- Deutzmann JS. 2020. Anaerobic methane oxidation in freshwater environments. In: Boll M, Ed. Anaerobic utilization of hydrocarbons, oils, and lipids: handbook of hydrocarbon and lipid microbiology. Cham: Springer. p 391–404.
- Doubek JP, Campbell KL, Doubek KM, Hamre KD, Lofton ME, McClure RP, Ward NK, Carey CC. 2018. The effects of hypolimnetic anoxia on the diel vertical migration of freshwater crustacean zooplankton. *Ecosphere* 9(7):e02332.
- Downing JA, Cole JJ, Middelburg JJ, Striegl RG, Duarte CM, Kortelainen P, Prairie YT, Laube KA. 2008. Sediment organic carbon burial in agriculturally eutrophic impoundments over the last century. *Global Biogeochem Cycles* 22:GB1018.
- Frintde K, Allgaier M, Grossart HP, Eckert W. 2015. Microbial response to experimentally controlled redox transitions at the sediment water interface. *PLoS One* 10(11):e0143428.
- Galand PE, Fritze H, Conrad R, Yrjälä K. 2005. Pathways for methanogenesis and diversity of methanogenic archaea in three boreal peatland ecosystems. *App Environ Micro* 71:2195–8.
- Gehring T, Klang J, Niedermayr A, Berzio S, Immenhauser A, Klocke M, Lübken M. 2015. Determination of methanogenic pathways through carbon isotope ( $\delta^{13}\text{C}$ ) analysis for the two-stage anaerobic digestion of high-solids substrates. *Environ Sci Tech* 49:4705–14.
- Gerling AB, Browne RG, Gantzer PA, Mobley MH, Little JC, Carey CC. 2014. First report of the successful operation of a side stream supersaturation hypolimnetic oxygenation system in a eutrophic, shallow reservoir. *Water Res* 67:129–43.
- Gerling AB, Munger ZW, Doubek JP, Hamre KD, Gantzer PA, Little JC, Carey CC. 2016. Whole-catchment manipulations of internal and external loading reveal the sensitivity of a century-old reservoir to hypoxia. *Ecosystems* 19:555–71.
- Hamre KD, Gerling AB, Munger ZW, Doubek JP, McClure RP, Cottingham KL, Carey CC. 2017. Spatial variation in dinoflagellate recruitment along a reservoir ecosystem continuum. *J Plankton Res* 39:715–28.
- Hamre KD, Lofton ME, McClure RP, Munger ZW, Doubek JP, Gerling AB, Schreiber ME, Carey CC. 2018. In situ fluorometry reveals a persistent, perennial hypolimnetic cyanobacterial bloom in a seasonally anoxic reservoir. *Freshw Sci* 37:483–95.
- Hartnett HE, Keil RG, Hedges JI, Devol AH. 1998. Influence of oxygen exposure time on organic carbon preservation in continental margin sediments. *Nature* 391:572–5.
- Huttunen JT, Hammar T, Alm J, Silvola J, Martikainen PJ. 2001. Greenhouse gases in non-oxygenated and artificially oxygenated eutrophied lakes during winter stratification. *J Environ Qual* 30:387–94.
- Jennings E, Jones S, Arvola L, Staehr PA, Gaiser E, Jones ID, Weathers KC, Weyhenmeyer GA, Chiu C, De Eyto E. 2012. Effects of weather-related episodic events in lakes: an analysis based on high-frequency data. *Freshw Biol* 57:589–601.
- Jenny JP, Francus P, Normandeau A, Lapointe F, Perga ME, Ojala A, Schimmelmann A, Zolitschka B. 2016. Global spread of hypoxia in freshwater ecosystems during the last three centuries is caused by rising local human pressure. *Glob Chang Biol* 22:1481–9.
- Jokinen S, Virtasalo JJ, Jilber TS, Kaiser J, Dellwig O, Arz HW, Hänninen J, Arppe L, Collander M, Saarinen T. 2018. A 1500-year multiproxy record of coastal hypoxia from the northern Baltic Sea indicates unprecedented deoxygenation over the 20th century. *Biogeosciences* 15:3975–4001.
- Kehew AE. 2000. Applied chemical hydrogeology. Upper Saddle River: Prentice Hall.
- Kelly CA, Rudd JW, Schindler DW. 1988. Carbon and electron flow via methanogenesis,  $\text{SO}_4^{2-}$ ,  $\text{NO}_3^-$ ,  $\text{Fe}^{3+}$ , and  $\text{Mn}^{4+}$  reduction in the anoxic hypolimnia of three lakes. *Arch Hydrobiol* 31:333–44.
- Klug JL, Richardson DC, Ewing HA, Hargreaves BR, Samal NR, Vachon D, Pierson DC, Lindsey AM, O’Donnell DM, Effler SW, Weathers KC. 2012. Ecosystem effects of a tropical cyclone on a network of lakes in northeastern North America. *Environ Sci Tech* 46:11693–701.

- Knoll LB, Vanni MJ, Renwick WH, Dittman EK, Gephart JA. 2013. Temperate reservoirs are large carbon sinks and small CO<sub>2</sub> sources: results from high-resolution carbon budgets. *Global Biogeochem Cycles* 27:52–64.
- Kreling J, Bravidor J, Engelhardt C, Hupfer M, Koschorreck M, Lorke A. 2017. The importance of physical transport and oxygen consumption for the development of a metalimnetic oxygen minimum in a lake. *Limnol Oceanogr* 62:348–63.
- Krueger KM, Vavrus CE, Lofton ME, McClure RP, Gantzer PA, Carey CC, Schreiber ME. 2020. Iron and manganese fluxes across the sediment-water interface in a drinking water reservoir. *Water Res.* 182:116003.
- Lau MP, Sander M, Gelbrecht J, Hupfer M. 2016. Spatiotemporal redox dynamics in a freshwater lake sediment under alternating oxygen availabilities: combined analyses of dissolved and particulate electron acceptors. *Environ Chem* 13:826–37.
- Lau MP, Sander M, Gelbrecht J, Hupfer M. 2015. Solid phases as important electron acceptors in freshwater organic sediments. *Biogeochemistry* 123:49–61.
- Marcè R, Rodríguez-Arias MÀ, García JC, Armengol J. 2010. El Niño Southern oscillation and climate trends impact reservoir water quality. *Glob Chang Biol* 16:2857–65.
- Matthews DA, Effler SW, Driscoll CT, O'Donnell SM, Matthews CM. 2008. Electron budgets for the hypolimnion of a recovering urban lake, 1989–2004: response to changes in organic carbon deposition and availability of electron acceptors. *Limnol Oceanogr* 53:743–59.
- Mattson MD, Likens GE. 1992. Redox reactions of organic matter decomposition in a soft water lake. *Biogeochemistry* 19:149–72.
- Matzinger A, Müller B, Niederhauser P, Schmid M, Wüest A. 2010. Hypolimnetic oxygen consumption by sediment-based reduced substances in former eutrophic lakes. *Limnol Oceanogr* 55:2073–84.
- Mayr MJ, Zimmermann M, Dey J, Brand A, Wehrli B, Bürgmann H. 2020. Growth and rapid succession of methanotrophs effectively limit methane release during lake overturn. *Communications Biol* 3:108.
- McClain ME, Boyer EW, Dent CL, Gergel SE, Grimm NB, Groffman PM, Hart SC, Harvey JW, Johnston CA, Mayorga E, McDowell WH, Pinay G. 2003. Biogeochemical hot spots and hot moments at the interface of terrestrial and aquatic ecosystems. *Ecosystems* 6:301–12.
- Mendonça R, Müller RA, Clow D, Verpoorter C, Raymond P, Tranvik LJ, Sobek S. 2017. Organic carbon burial in global lakes and reservoirs. *Nat Commun* 8:1–7.
- McClure RP, Hamre KD, Niederlehner BR, Munger ZW, Chen S, Lofton ME, Schreiber ME, Carey CC. 2018. Metalimnetic oxygen minima alter the vertical profiles of carbon dioxide and methane in a managed freshwater reservoir. *Sci Total Environ* 636:610–20.
- Munger ZW, Carey CC, Gerling AB, Hamre KD, Doubek JP, Klepazki SD, McClure RM, Schreiber ME. 2016. Effectiveness of hypolimnetic oxygenation for preventing accumulation of Fe and Mn in a drinking water reservoir. *Water Res* 106:1–14.
- Munger ZW, Carey CC, Gerling AB, Doubek JP, Hamre KD, McClure RP, Schreiber ME. 2019. Oxygenation and hydrologic controls on iron and manganese mass budgets in a drinking-water reservoir. *Lake Reservoir Manag* 35:277–91.
- Morris JC, Stumm W. 1967. Redox equilibria and measurements of potentials in the aquatic environment. In: *Equilibrium concepts in natural water systems*. pp 270–85.
- Oswald K, Milucka J, Brand A, Littmann S, Wehrli B, Kuypers MM, Schubert CJ. 2015. Light-dependent aerobic methane oxidation reduces methane emissions from seasonally stratified lakes. *PLoS One* 10(7):e0132574.
- Picardal F. 2012. Abiotic and microbial interactions during anaerobic transformations of Fe(II) and NO<sub>x</sub>. *Frontiers Microbiol* 3:112.
- Peeters F, Fernandez JE, Hofmann H. 2019. Sediment fluxes rather than oxic methanogenesis explain diffusive CH<sub>4</sub> emissions from lakes and reservoirs. *Sci Rep* 9:1–10.
- Prairie YT, Alm J, Beaulieu J, Barros N, Battin T, Cole JJ, del Giorgio P, DelSontro T, Guérin F, Harby A, Harrison J, Mercier-Blais S, Serça D, Sobek S, Vachon D. 2018. Greenhouse gas emissions from freshwater reservoirs: What does the atmosphere see? *Ecosystems* 21:1058–71.
- Read JS, Hamilton DP, Jones ID, Muraoka K, Winslow LA, Kroiss R, Wu CH, Gaiser E. 2011. Derivation of lake mixing and stratification indices from high-resolution lake buoy data. *Env Model Softw* 26:1325–36.
- Rudd JW, Hamilton RD. 1978. Methane cycling in a eutrophic shield lake and its effects on whole lake metabolism. *Limnol Oceanogr* 23:337–48.
- Schafran GC, Driscoll CT. 1987. Comparison of terrestrial and hypolimnetic sediment generation of acid neutralizing capacity for an acidic Adirondack lake. *Environ Sci Tech* 21:988–93.
- Schindler DW. 1998. Whole-ecosystem experiments: replication versus realism: the need for ecosystem-scale experiments. *Ecosystems* 1:323–34.
- Schlesinger WH. 1997. *Biogeochemistry: an analysis of global change*. 2nd edn. San Diego (CA): Academic Press. p 588.
- Sivan O, Adler M, Pearson A, Gelman F, Bar-Or I, John SG, Eckert W. 2011. Geochemical evidence for iron-mediated anaerobic oxidation of methane. *Limnol Oceanogr* 56:1536–44.
- Sobek S, Durisch-Kaiser E, Zurbrügg R, Wongfun N, Wessels M, Pasche N, Wehrli B. 2009. Organic carbon burial efficiency in lake sediments controlled by oxygen exposure time and sediment source. *Limnol Oceanogr* 54:2243–54.
- Stanley EH, Casson NJ, Christel ST, Crawford JT, Loken LC, Oliver SK. 2016. The ecology of methane in streams and rivers: patterns, controls, and global significance. *Ecol Monogr* 86:146–71.
- Stumm W, Morgan JJ. 1996. *Aquatic chemistry*. 3rd edn. New York (NY): Wiley. p 1040.
- Tranvik LJ, Downing JA, Cotner JB, Loiselle SA, Striegl RG, Ballatore TJ, Dillon P, Finlay K, Fortino K, Knoll LB, Kortelainen PL, Kuster T, Larsen S, Laurion I, Leech DM, McCallister SL, McKnight DM, Melak JM, Overholt E, Porter JA, Prairie Y, Renwick WH, Roland F, Sherman BS, Schindler DW, Sobek S, Tremblay A, Vanni MJ, Verschoor AM, Wachenfeldt E, Weyhenmeyer GA. 2009. Lakes and reservoirs as regulators of carbon cycling and climate. *Limnol Oceanogr* 54(6part2):2298–314.
- Vegas-Vilarrúbia T, Corella JP, Pérez-Zanón N, Buchaca T, Trapote MC, López P, Sigró J, Rull V. 2018. Historical shifts in

- oxygenation regime as recorded in the laminated sediments of lake Montcortès (Central Pyrenees) support hypoxia as a continental-scale phenomenon. *Sci Total Environ* 612:1577–92.
- Viollier E, Inglett PW, Hunter K, Roychoudhury AN, Van Cappellen P. 2000. The ferrozine method revisited: Fe(II)/Fe(III) determination in natural waters. *J Appl Geochem* 15:785–90.
- Virginia Division of Mineral Resources. 2003. Digital representation of the 1993 geologic map of Virginia, Publication 174, CD ROM (ISO-9660) contains image file, expanded explanation in pdf, and ESRI shapefiles, scale 1:500000.
- US EPA. 1994. Method 200.7: determination of metals and trace elements in water and wastes by inductively coupled plasma-atomic emission spectrometry.
- Weathers KC, Stayer DL. 2013. Fundamentals of ecosystem science. In: Appendix—A primer in biologically mediated redox reactions in ecosystems. pp 297–301.
- Wilkinson GM, Cole JJ, Pace ML, Johnson RA, Kleinmans MJ. 2015. Physical and biological contributions to metalimnetic oxygen maxima in lakes. *Limnol Oceanogr* 60:242–51.